JACS
JOURNAL OF THE AMERICAN CHEMICAL SOCIETY
Article
pubs.acs.org/JACS

Tetrathiafulvalene-Based Nanotweezers—Noncovalent Binding of Carbon Nanotubes in Aqueous Media with Charge Transfer Implications

Carlos Romero-Nieto,[†] Raúl García,[‡] M. Ángeles Herranz,[‡] Christian Ehli,[†] Michaela Ruppert,[§] Andreas Hirsch,*[,§] Dirk M. Guldi,*[,†] and Nazario Martín*[,‡,∥]

[†]Department of Chemistry and Pharmacy & Interdisciplinary Center for Molecular Materials (ICMM), Friedrich-Alexander-Universität Erlangen-Nürnberg, Egerlandstrasse 3, 91058 Erlangen, Germany

[‡]Departamento de Química Orgánica, Facultad de Química, Universidad Complutense de Madrid, 28040 Madrid, Spain

[§]Department of Chemistry and Pharmacy, Friedrich-Alexander-Universität Erlangen-Nürnberg, Henkestrasse 42, 91054 Erlangen, Germany

[∥]IMDEA-Nanoscience, Campus de Cantoblanco, 28049 Madrid, Spain

Supporting Information

ABSTRACT: Electron donor–acceptor hybrids based on single wall carbon nanotubes (SWCNT) are one of the most promising functional structures that are currently developed in the emerging areas of energy conversion schemes and molecular electronics. As a suitable electron donor, π-extended tetrathiafulvalene (exTTF) stands out owing to its recognition of SWCNT through $\pi-\pi$ stacking and electron donor–acceptor interactions. Herein, we explore the shape and electronic complementarity between different types of carbon nanotubes (CNT) and a tweezers-shaped molecule endowed with two exTTFs in water. The efficient electronic communication between semiconducting SWCNT/multiwall carbon nanotubes (MWCNT), on one hand, and the water-soluble exTTF nanotweezers **8**, on the other hand, has been demonstrated in the ground and excited state by using steady-state as well as time-resolved spectroscopies, which were further complemented by microscopy. Importantly, appreciable electronic communication results in the electronic ground state having a shift of electron density, that is, from exTTFs to CNT, and in the electronic excited state having a full separation of electron density, that is oxidized exTTF and reduced CNT. Lifetimes in the range of several hundred picoseconds, which were observed for the corresponding electron transfer products upon light irradiation, tend to be appreciably longer in MWCNT/**8** than in SWCNT/**8**.

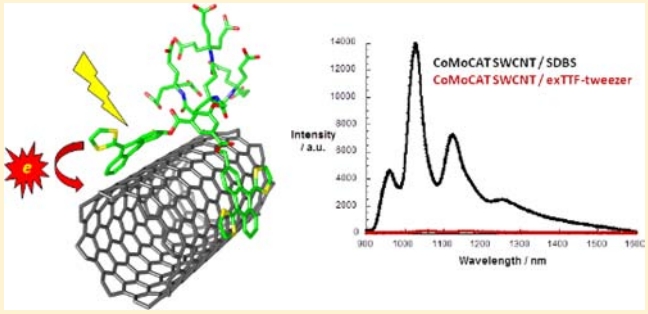

INTRODUCTION

In the past decade, an entire area of research has focused on the chemistry of carbon nanotubes (CNT), in general, and of single wall carbon nanotubes (SWCNT), in particular.[1] CNT possess unique structural, electronic, mechanical, and optical properties that render them ideal components for emerging fields,[2] such as field-effect transistors (FETs),[3] light-emitting diodes (LEDs),[4] organic solar cells (OSCs),[5] water oxidation,[6] biochemical sensors,[7] and memory elements,[8] or as additives in advanced composite materials.[9]

Most of these applications are, however, tied to the intrinsic manipulation of CNT and/or interaction with materials that should be performed either in solutions or in highly viscous matrices. The poor solubility of CNT in common media, aqueous or organic solvents, often hinders their processability. Here, the large bundles that originate from attractive interactions such as $\pi-\pi$ stacking and London dispersion forces are aspects that require careful attention. In this respect, the chemical modification of CNT has emerged as a powerful approach to overcome some of the bottlenecks that are associated with the lack of processability.[10] A real asset is the noncovalent functionalization of CNT as it assists in improving the solubility without, however, impacting the electronic structure.[11] Up to now, a myriad of versatile methodologies that ensure the processability of CNT in organic solvents have been established.[12] However, analogous methodologies for processing them in aqueous media and for realizing water-soluble electron donor–acceptor hybrids still remain scarce.

Crucial for device applications is to explore the electronic interactions of small molecules[13] or polymers[14] with CNT. To this end, the use of molecules that feature nanotweezers-like

Received: December 5, 2011
Published: May 11, 2012

   dx.doi.org/10.1021/ja211362z | J. Am. Chem. Soc. 2012, 134, 9183–9192

geometries appears promising. In such nanotweezers the presence of two or more aromatic groups is essential to ensure efficient and selective bindings by noncovalent interactions. Likewise, those aromatic moieties offer, additionally, the possibility to investigate the electronic communication with CNT. Some particularly interesting examples of nanotweezers-like geometries that have been shown to bind SWCNT include pentacenes or dihydronaphthopentaphenes that are bridged by a rigid core.[15,16] In a similar manner, the nanotweezers concept has been also expanded to 1- and 2-pyrene pincers[17] as well as to chiral diporphyrins.[18] Recently, the optimization of the nanotweezers structure resulted in a simultaneous discrimination of handedness and diameter, which altogether enabled enriching (6,5) SWCNT as single enantiomers.[19] On the basis of the ability of water-soluble perylene surfactants to disperse and individualize CNT,[20] some of us have successfully implemented perylene-based nanotweezers as a means to selectively interact with larger diameter SWCNT.[21]

A fascinating building block for the construction of nanotweezers is π-extended tetrathiafulvalene (exTTF).[22] This proaromatic compound reveals high affinity toward carbon nanomaterials. For example, binding constants of fullerenes, in a variety of solvents and at variable temperatures, are in the log K_a range from 3 to 4.[23] Important is also the fact that electronic interactions between exTTF and SWCNT, in the form of photoinduced electron transfer, have already been corroborated with a pyrene appended exTTF.[24]

Motivated by the aforementioned, we designed the exTTF nanotweezers **8** (Scheme 1) for probing noncovalent interactions with different types of CNT (i.e., HiPco SWCNT, CoMoCAT SWCNT, and multiwall carbon nanotubes (MWCNT)) in aqueous media. Importantly, **8** bears two exTTFs as anchors that are connected by a flexible linkage, allowing a priory for size-adaptable interactions with CNT of different diameters. In addition, **8** was designed to combine the two exTTF anchors with a hydrophilic dendron of second generation with terminal carboxylic groups. Deprotonation of the latter in basic media warrants its solubility in water and, at the same time, its exfoliating character of individual CNT. As a matter of fact, complementary assays by means of microscopy and spectroscopy documented that **8** is suitable for the noncovalent functionalization of CNT in aqueous media. Most importantly, ground and excited state interactions between CNT and **8** were unequivocally proven.

RESULTS AND DISCUSSION

Synthesis and Sample Preparation. The multistep synthesis of exTTF nanotweezers **8** is summarized in Scheme 1. Starting from the exTTF derivative **1**[25] and following a modification of a previously reported procedure,[26] the esterification with **2** in the presence of *N*-(3-dimethylaminopropyl)-*N*′-ethylcarbodiimide hydrochloride (EDC) and 4-dimethylaminopyridine (DMAP), followed by deprotection of the *tert*-butyldimethylsilyl (TBDMS) group led to **4** with an excellent overall yield. After reacting **4** with *tert*-butylbromoacetate, the isolated ester **5** was reacted with the corresponding dendritic amine **6**.[27] In doing so, the terminal ester groups of **5** were initially hydrolyzed with formic acid, followed by a condensation reaction with **6** in the presence of *N*,*N*′-dicyclohexylcarbodiimide (DCC), *N*-hydroxybenzotriazole (HOBt), and DMAP to yield **7**. The water-soluble nanotweezer **8** was finally generated by a nearly quantitative acidic cleavage of the peripheral *tert*-butyl groups of **7**. The novel exTTF

Scheme 1. Synthesis of exTTF Nanotweezers 8 as Well as the Corresponding Precursors 3, 4, 5, and 7[a]

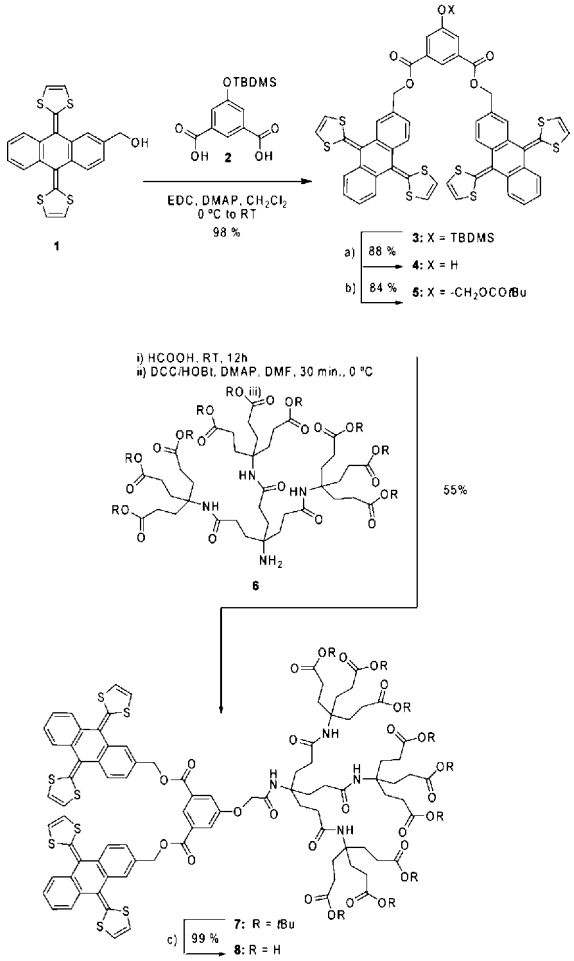

[a]Conditions: (a) Bu_4NF, THF, RT; (b) *tert*-butylbromoacetate, acetone, and K_2CO_3, 5 h reflux; (c) HCOOH, RT, 3 days.

nanotweezer **8** and its precursors, **3**–**5** and **7**, have been fully characterized by common spectroscopic techniques. Additional details are gathered in the Experimental Section.

The CNT/exTTF nanotweezers hybrids were prepared by mixing 0.5 mg of the corresponding CNT and 1 mg of **8** in a 0.1 M borax aqueous solution. In a first and second step, the dispersions and the resulting supernatants, respectively, were kept for 12 h under vigorous stirring, sonicated for 45 min at 20 °C, and, finally, centrifuged (i.e., 15 min at 8000 rpm) to remove large bundles. In the final step, the supernatant was collected and the stirring/sonication/centrifugation cycle was repeated but with 5 min of centrifugation at 12000 rpm. Prior to optical measurements (i.e., emission and pump probe), the optical density of the dark grayish supernatant was adjusted to meet the specific requirements.

Microscopic Characterization of CNT/8. An important structural feature of **8** is the dendron of second generation that carries peripheral carboxylic acid groups. The peripheral carboxylic acid groups render **8** soluble in 0.1 M borax solutions. With a solution of **8** in hand, aqueous solutions of different CNT were prepared. In terms of stability, MWCNT/**8** suspensions were found to be stable for months, while suspensions of CoMoCAT SWCNT/**8** and HiPco SWCNT/

dx.doi.org/10.1021/ja211362z | J. Am. Chem. Soc. 2012, 134, 9183–9192

8 exhibited stabilities that lasted for weeks and days, respectively.

Initially, atomic force microscopy (AFM) was employed to confirm the presence of exfoliated SWCNT/**8** on, for example, a drop-casted silicon wafer (Figure 1). After deposition, the

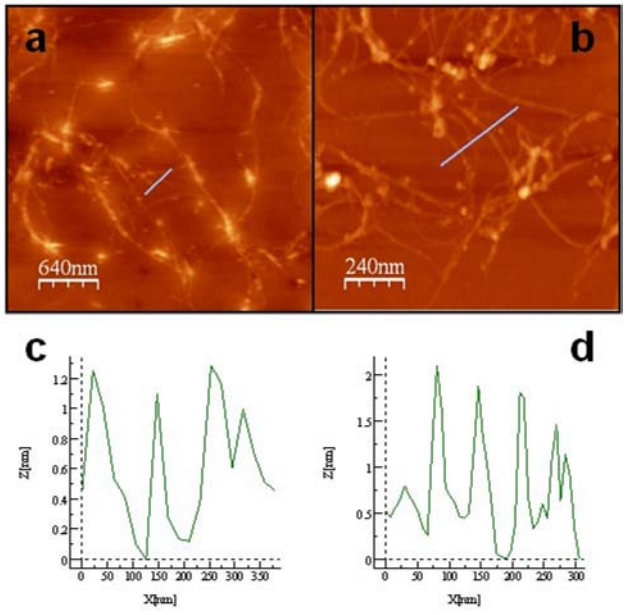

Figure 1. (a) Representative AFM image of HiPco SWCNT/**8** with a scale bar of 640 nm. (b) Representative AFM image of CoMoCAT SWCNT/**8** with a scale bar of 240 nm. (c and d) Corresponding height profiles.

wafers were washed with deionized water to minimize the interference of borax crystals in the AFM images. Overall, similar features were observed for both types of nanohybrids, namely HiPco SWCNT/**8** and CoMoCAT SWCNT/**8**. Typical images reveal, for example, that the SWCNT/**8** suspensions consist of well isolated and individual SWCNT that arise together with a few small bundles. The latter coexist, however, with a few remaining borax nanocrystals. A distribution of hybrids with lengths of several micrometers and diameters of 0.8−1.4 nm was seen throughout the scanned areas. This fact points unambiguously to the successful immobilization of **8** onto SWCNT, which, in turn, ensures disaggregated SWCNT/**8** nanohybrids.

To complement the aforementioned AFM investigations, we turned to transmission electron microscopy (TEM) (Figure 2 and Supporting Information Figure S1). In line with the AFM measurements, detailed analyses of, for example, CoMoCAT and HiPco SWCNT nanohybrids revealed the presence of individual SWCNT that coexist with smaller SWCNT bundles (i.e., up to 3.5 nm). In particular, comparing the diameter distributions of CoMoCAT and HiPco SWCNT, wrapped with either sodium dodecyl benzene sulfonate (SDBS) or with **8**, corroborates the AFM investigations (see the statistical analysis in Supporting Information Figure S2). The presence of **8** is seen in additionally recorded HRTEM images in the form of an amorphous SWCNT coating (Figure 3).

In addition, the flexibility of the ester linkages was thought to confer the capability of **8** to assemble CNT of even larger diameters than in SWCNT. With this in mind, we ran tests with MWCNT, which are known to have considerably larger

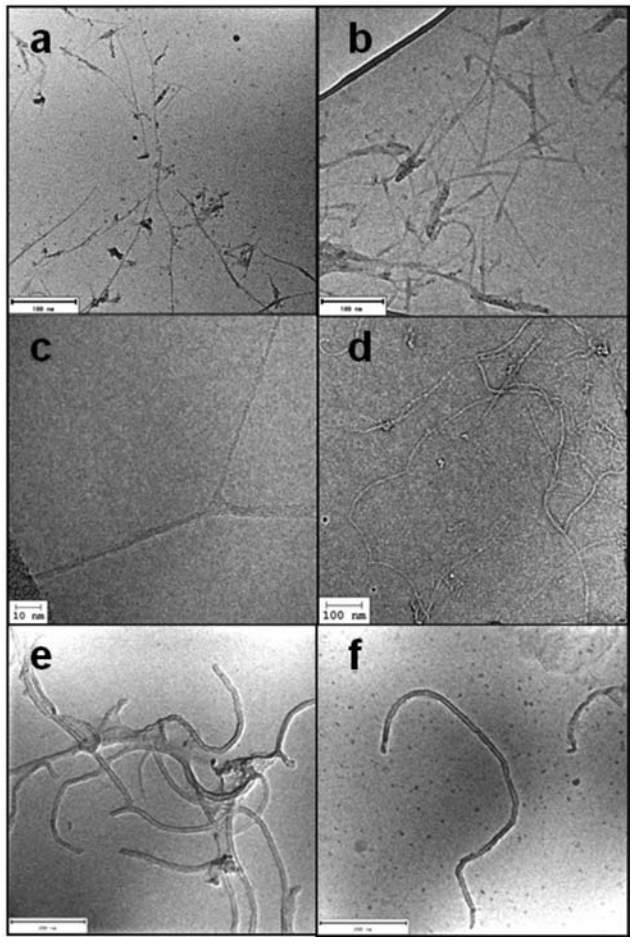

Figure 2. (a and b) Representative TEM images of HiPco SWCNT/**8** on holey carbon grids with scale bars of 100 nm. (c and d) Representative TEM images of CoMoCAT SWCNT/**8** on holey carbon grids with scale bars of 10 and 100 nm, respectively. (e and f) Representative TEM images of MWCNT/**8** on standard Formvar film coated copper grids with scale bars of 200 nm.

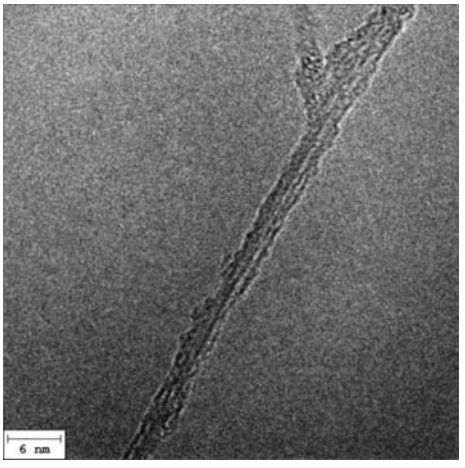

Figure 3. Representative HRTEM image of CoMoCAT SWCNT/**8** with a scale bar of 6 nm.

diameters than SWCNT. Indeed, by following a similar procedure, that is, employing borax aqueous solutions, MWCNT/**8** suspensions were successfully obtained. Interestingly, as mentioned above, these suspensions were stable for

dx.doi.org/10.1021/ja211362z | J. Am. Chem. Soc. 2012, 134, 9183−9192

months without giving rise to any appreciable decomposition. The microscopic investigations by means of TEM revealed also in this case a high degree of well dispersed MWCNT (Figure 2). These are wrapped with uniform layers of amorphous **8**. Notably, only a slightly larger mean diameter was observed when comparing the diameters of MWCNT/**8** nanohybrids (11.6 nm) with those of MWCNT/SDBS (11.1 nm) prepared under the same conditions (see Supporting Information Figure S2). These results clearly corroborate the versatility of the designed nanotweezers to interact not only with different types of SWCNT but also with larger diameter MWCNT.

Spectroscopic Characterization of CNT/8. Ensuring homogenously dispersed CNT suspensions has emerged as a necessity in the field of CNT. It is, however, insufficient for deducing information about the electronic communications between CNT, on one hand, and exTTF nanotweezers, on the other hand. An unambiguous clarification mandates performing detailed spectroscopic investigations.

In doing so, aqueous suspensions of SWCNT/**8** were tested initially by absorption spectroscopy. When compared to HiPco SWCNT that were suspended by SDBS, all of the absorption features of the HiPco SWCNT/**8** nanohybrids give rise to a marked red-shift (Figure 4). In particular, the E_{22} absorption peaks of HiPco SWCNT undergo a weak but notable bathochromic shift (from 552, 594, 644, 729, 800, and 862 nm to 558, 602, 653, 739, 810, and 875 nm). Much larger are the shifts in the E_{11} absorption peaks of HiPco SWCNT (from 1117, 1171, 1265, and 1410 nm to 1147, 1211, 1294, and 1442 nm). We imply appreciable electron donor−acceptor interactions in SWCNT/**8** between the electron donating exTTF nanotweezers and SWCNT that increase the electron density in the SWCNT conduction bands and, in turn, lower the transition energy.[13,20]

A similar trend was noted for the CoMoCAT SWCNT/**8** nanohybrids. Here, the features of the E_{11} absorption peaks of CoMoCAT SWCNT red-shifted from 980, 1025, 1155, and 1265 nm in the case of CoMoCAT SWCNT/SDBS to 1005, 1055, 1155, and 1295 nm in the case of CoMoCAT SWCNT/**8**. On the other hand, the E_{22} absorption peaks in CoMoCAT SWCNT/SDBS at 450, 500, 570, 590, 650, and 725 nm were only marginally impacted by the presence of **8** with red-shifts that are on the order of a few nanometers. Interesting is the fact that the relative intensities are not altered upon suspending SWCNT with **8**. This prompts the conclusion that **8** reveals, among the semiconducting SWCNT present, no particular preference during the suspension. The reversible immobilization of **8** was confirmed by subsequent addition of SDBS (Figure 4), which resulted in a quantitative restore of the intrinsic CoMoCAT SWCNT features.

Notably, MWCNT absorption spectra, even when SDBS is employed as a surface active stabilizer, are typically structureless and give rise to an asymptotic decrease of intensity toward the near-infrared. The latter hampered, however, detailed analyses of the impact that immobilization of **8** exerts on the electronic structure (Supporting Information Figure S3).

Next, the fluorescence features of the HiPco and CoMoCAT SWCNT/**8** nanohybrids were investigated. In particular, HiPco SWCNT/**8** display E_{11} fluorescence maxima at 1080, 1141, 1215, 1300, and 1422 nm (Figure 5). It is important to note that the fluorescent features mirror image the ground state

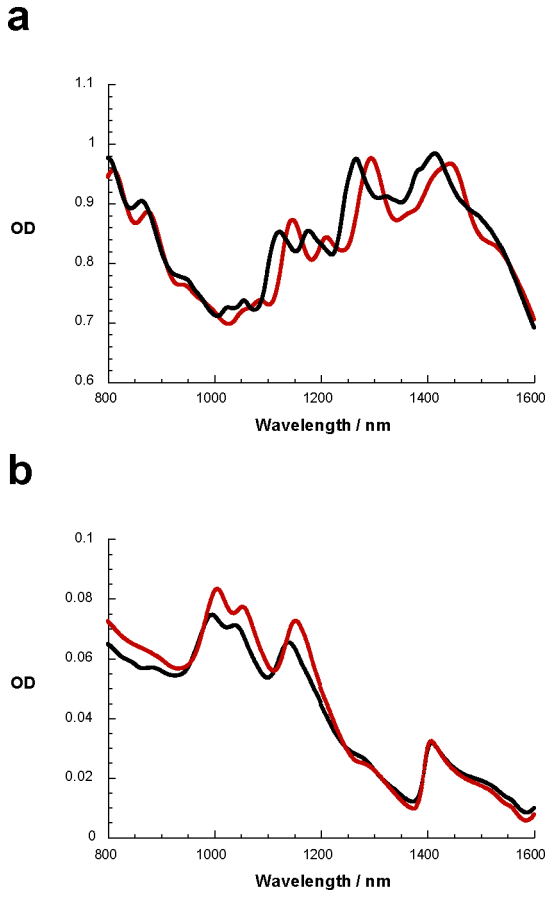

Figure 4. (a) Absorption spectra of HiPco SWCNT/SDBS (black spectrum) and HiPco SWCNT/**8** (red spectrum) in D_2O. (b) Absorption spectra of CoMoCAT SWCNT/SDBS (black spectrum) and CoMoCAT SWCNT/**8** (red spectrum).

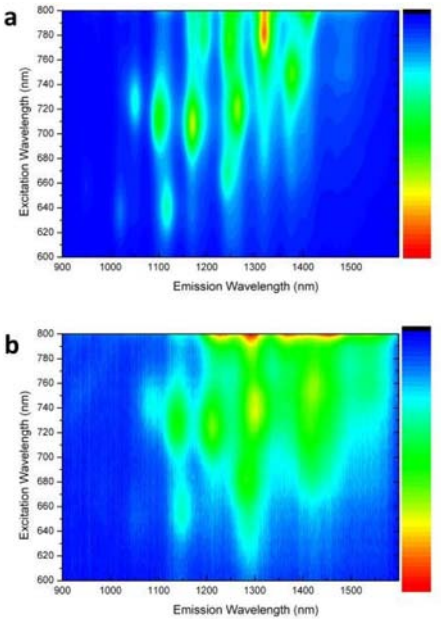

Figure 5. (a) 3D steady-state fluorescence spectra, with increasing intensity from blue to green to yellow and to red, of HiPco SWCNT/SDBS in D_2O. (b) 3D steady-state fluorescence spectra, with increasing intensity from blue to green to yellow and to red, of HiPco SWCNT/**8** in D_2O. Please note the lower spectra have been amplified by a factor of 21.

dx.doi.org/10.1021/ja211362z | J. Am. Chem. Soc. 2012, 134, 9183−9192

absorption. Contrasting the fluorescence of the SWCNT/**8** nanohybrids with that of SWCNT/SDBS at equal absorbances at the excitation wavelength sheds light onto the mutual interactions via either radiative or nonradiative decays in SWCNT/**8** (Supporting Information Figure S4). To this end, HiPco SWCNT/**8** reveals an energetic shift of the fluorescent transitions in the form of red-shifted maxima relative to those seen for HiPco SWCNT/SDBS. For HiPco SWCNT/SDBS, maxima at 1054, 1103, 1174, 1268, 1322, and 1376 nm were measured, which correspond to (10,2), (9,4), (8,6), (8,7), (9,7), and (10,6) SWCNT, respectively.[28] Again, a redistribution of electron density from the electron donor to the SWCNT conduction bands is responsible for this shift to lower energies. Examination of the fluorescence intensities (Supporting Information Figure S4) prompts up to a 71% quenching of the HiPco SWCNT features. Hereby, the high energy transitions (i.e., 1080 nm) are more strongly quenched than the medium energy transitions (i.e., 1141, 1215, and 1300 nm) and the low energy transitions (i.e., 1422 nm). We imply the occurrence of nonradiative singlet excited state deactivations in HiPco SWCNT/**8** such as energy and/or electron transfer. Bundling/rebundling, on the other hand, as it may lead to SWCNT fluorescence quenching, is ruled out on the basis of the AFM and TEM studies (vide supra). In addition, we have no evidence for energy transfer between different SWCNT.

The fluorescence of CoMoCAT SWCNT/**8** evolves at 990, 1055, 1158, and 1300 nm (Figures 6 and 7). They are in the same way red-shifted, as seen for HiPco SWCNT. For example, the corresponding maxima appear for CoMoCAT SWCNT/SDBS at 958, 1028, 1125, and 1250 nm, which are attributed to (8,3), (7,5), (7,6), and (8,7) SWCNT.[28] At first glance, when comparing the fluorescence intensity of CoMoCAT SWCNT/**8** with that of CoMoCAT SWCNT/SDBS exhibiting both equal absorbance at the excitation wavelength, a significant quenching is noted. The quenching is as strong as 99% (Figure 7). A closer analysis reveals that the quenching for the high energy features, that is at 990/1055 nm, is more than twice as strong as that for the medium energy feature at 1158 nm and nearly three times as strong as that for the low energy feature at 1300 nm. This observation goes hand in hand with the altered redox properties of different SWCNT that relate to their size confinement.

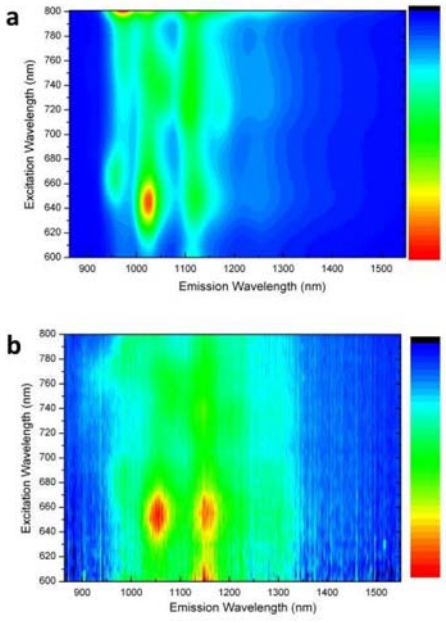

Figure 6. (a) 3D steady-state fluorescence spectra, with increasing intensity from blue to green to yellow and to red, of CoMoCAT SWCNT/SDBS in D_2O. (b) 3D steady-state fluorescence spectra, with increasing intensity from blue to green to yellow and to red, of CoMoCAT SWCNT/**8** in D_2O. Please note the lower spectra have been amplified by a factor of 88.

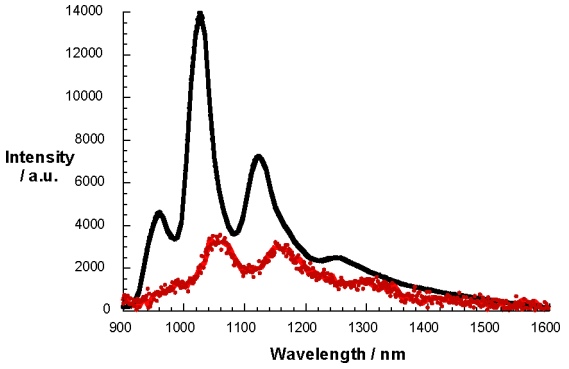

Figure 7. Comparison of the NIR fluorescence spectra of CoMoCAT SWCNT/SDBS (black spectrum) and CoMoCAT SWCNT/**8** (red spectrum) amplified by a factor of 20 in D_2O: 651 nm excitation.

Insights into CNT/exTTF electronic interactions came from RAMAN experiments.[29] Here, the three most important signatures, that is, RBM-, D-, and G-modes, reveal upshifts in D_2O suspensions of SWCNT/SDBS with respect to SWCNT/**8** as well as in the solid without evidencing loss in resonance. For example, the G-mode of both HiPco and CoMoCAT SWCNT shifts from 1590 ± 2 to 1592 ± 2 cm^{-1} (Figure 8). This indicates the fact that $\pi-\pi$ interactions are operative between SWCNT and **8**. Augmentation through ground state charge transfer/doping seems to play only a minor role. For MWCNT/**8**, only the RBM modes are subject to any notable shifts, that is, a downshift relative to MWCNT/SDBS. In addition, a new shoulder at around 1611 cm^{-1} develops (not shown).

In the final part of our investigations, transient absorption spectroscopy was employed. This was meant to determine the dynamics of the ultrafast singlet excited state deactivation in CNT/**8**, which was inferred from the fluorescence assays (vide supra). In addition, the experiments shed valuable light onto the characterization of the products evolving from interacting CNT and **8**.

In reference experiments, photoexcitation of **8** was probed at 387 nm (Supporting Information Figure S5). An exTTF centered excited state is generated with spectral characteristics that include transient maxima around 465, 650, and 990 nm as well as transient bleaching at <450 nm. An overall short lifetime of less than 2 ps is rationalized, in line with previous reports on the basis of the sulfur atoms, which impose a strong second-order vibronic spin−orbit coupling.[22]

We started our SWCNT investigations with HiPco SWCNT, that is, comparing HiPco SWCNT/SDBS with HiPco SWCNT/**8** upon 387 nm photoexcitation (Supporting Information Figures S6 and S7). The baseline is in the case of HiPco SWCNT/SDBS replaced with a strong bleaching that dominates the differential absorption spectra throughout the visible and near-infrared regions, where absorptive transitions of semiconducting SWCNT appear, respectively.[24] The major minima are seen at 975, 1020, 1135, and 1260 nm.

dx.doi.org/10.1021/ja211362z | J. Am. Chem. Soc. 2012, 134, 9183−9192

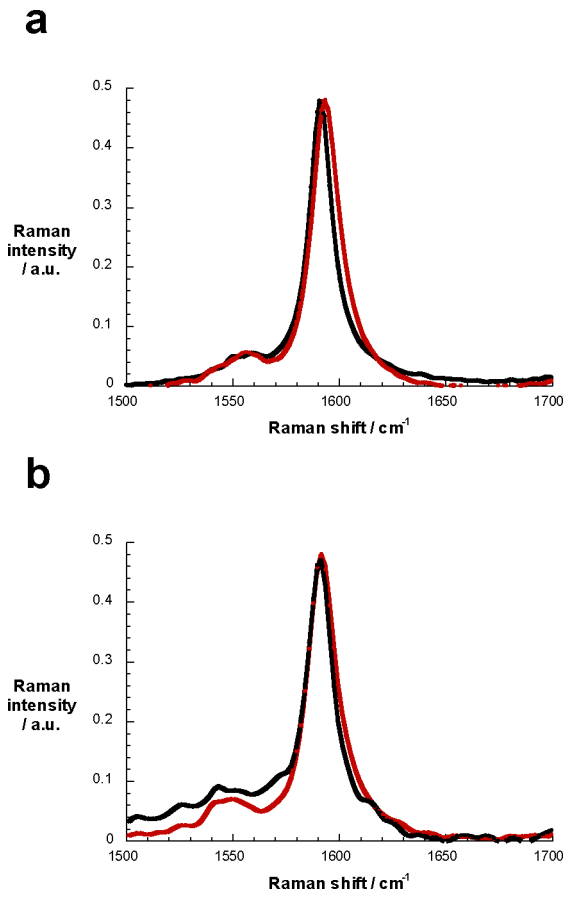

Figure 8. (a) Raman spectra of HiPco SWCNT/SDBS (black spectrum) and HiPco SWCNT/**8** (red spectrum) in D_2O suspensions: 1064 nm excitation. (b) Raman spectra of CoMoCAT SWCNT/SDBS (black spectrum) and CoMoCAT SWCNT/**8** (red spectrum) in D_2O suspensions: 1064 nm excitation.

Multiwavelength analyses of the bleaching characteristics in the near-infrared resulted in complex dynamics with two dominant lifetimes, namely 1.2 and 520 ps. Throughout these multiexponential decays the original absorption/baseline is quantitatively reinstated. Hereby, the polydisperse nature of HiPco SWCNT evokes a superimposition of a series of bleaching features. The latter correlate with individual SWCNT that absorb in nearly the same energetic range.

When turning to HiPco SWCNT/**8**, conditions were chosen that guaranteed stable SWCNT suspensions. In particular, a slight excess of **8** was essential. Interesting is the fact that the initial bleaching follows the trend seen in the absorption and fluorescence assays. To this end, minima and shoulders at 960, 1160, 1210, and 1300 nm reflect the overall red-shifts (Supporting Information Figure S7). In photoexcited HiPco SWCNT/**8**, these transient characteristics are metastable. In fact, lifetimes of 0.8 and 120 ps were derived from a multiwavelength analysis, which strongly evoke charge separation and charge recombination. Unlike CoMoCAT SWCNT/**8**—vide infra—spectroscopic evidence neither for the one electron radical cation of exTTF nor for the reduction of SWCNT was, however, gathered.

For CoMoCAT SWCNT/SDBS we noted in complementary transient absorption measurements negative differential absorption changes that resemble the ground state features (Figure 9). Immediately (i.e., 1 ps) upon femtosecond excitation, minima

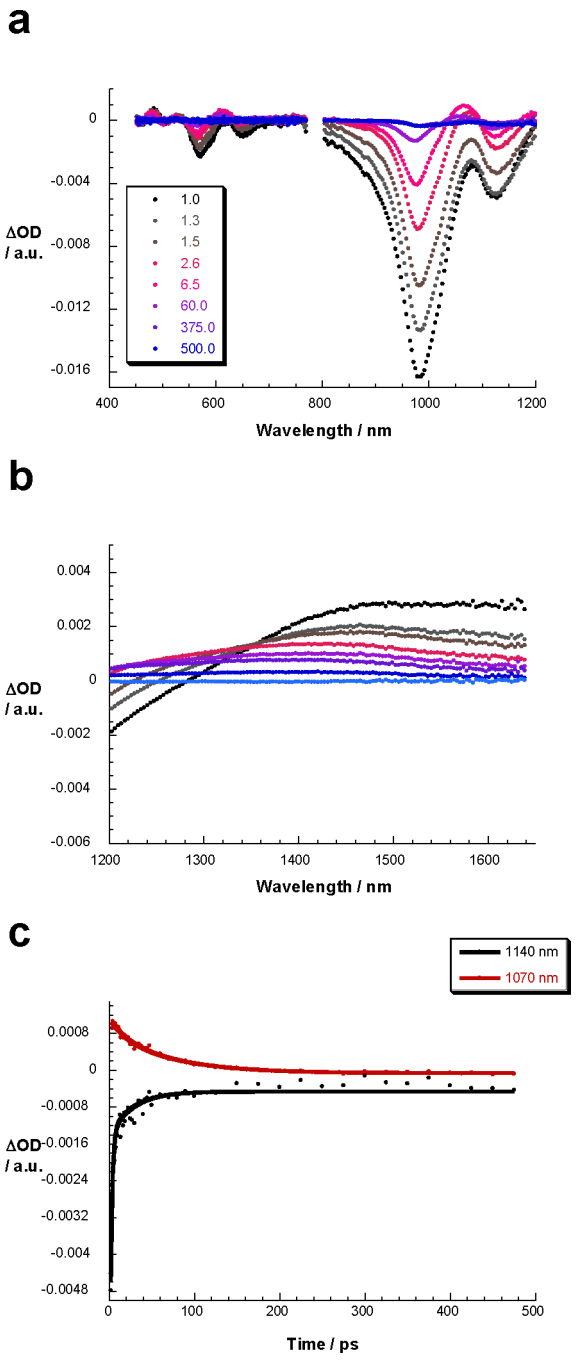

Figure 9. (a) Differential absorption spectra (visible and near-infrared) obtained upon femtosecond pump probe experiments (387 nm) of CoMoCAT SWCNT/SDBS in D_2O with several time delays between 1.1 and 500 ps at room temperature. (b) Differential absorption spectra (extended near-infrared) obtained upon femtosecond pump probe experiments (387 nm) of CoMoCAT SWCNT/SDBS in D_2O with several time delays between 1.1 and 500 ps at room temperature. (c) Time absorption profiles of the spectra shown in the upper part at 1140 (black spectrum) and 1070 nm (red spectrum) monitoring the excited state decay.

in the visible range at 570, 590, 650, and 725 nm and minima in the near-infrared range at 985 and 1130 nm correspond to a change of oscillator strength in SWCNT. In addition, shoulders at 1025 and 1270 nm and a maximum at 1465 nm were seen to develop. The decay of CoMoCAT SWCNT/SDBS excited states is fast and multiexponential. In fact, within 750 ps upon

dx.doi.org/10.1021/ja211362z | J. Am. Chem. Soc. 2012, 134, 9183–9192

photoexcitation all of the features decay. Two lifetimes of 0.6 and 68 ps dominate the dynamics, indicating ground state recovery (Figure 9). In line with previous investigations, the formation of new maxima (i.e., featuring positive differential absorption changes) at 485, 530, 610, 1065, 1215, and 1357 nm is associated with the transformation of the short-lived transient into the long-lived species.[30] In stark contrast to HiPco SWCNT—vide supra—the narrower distribution of CoMoCAT SWCNT enables the formation of positive differential absorption changes. The minima—with the exception of those at 650 and 985 nm—are, however, not susceptible to any appreciable changes during the ground state recovery.

Following photoexcitation of CoMoCAT SWCNT/**8** at 387 nm, we see in line with the absorption spectra the rapid formation of transient bleach at 590, 655, and 725 nm as well as at 1005, 1050, 1155, and 1295 nm due to semiconducting SWCNT (Figure 10). Notable are also red-shifts of the differential absorption changes when compared to the case of CoMoCAT SWCNT/SDBS. Again, this trend mirror images the differences in the absorption spectra of CoMoCAT SWCNT/**8** and CoMoCAT SWCNT/SDBS. The aforementioned attests the selective excitation of CoMoCAT SWCNT. The latter transforms, however, with a lifetime of 2.5 ps into a new transient. This newly formed transient reveals in the visible range a broad maximum at 680 nm, which resembles the radiolytically and photolytically generated fingerprint of the one electron oxidized radical cation of exTTF (Supporting Information Figure S8).[31] In the near-infrared, as time progresses, appreciable blue-shifts of the transient bleaches are detected, with minima that shift from 1005, 1050, 1155, and 1295 nm to 990, 1020, 1130, and 1250 nm, respectively. Notable is the lack of evidence for the long-lived species seen for CoMoCAT SWCNT/SDBS with its fingerprints at 1065, 1215, and 1357 nm—vide supra. Implicit are new conduction band electrons—injected from the exTTF—shifting the transitions to lower energies. Spectroelectrochemical reduction of CoMoCAT SWCNT/SDBS (Supporting Information Figure S9) further supports this notion. Taking the aforementioned into account, we conclude that the selective excitation of SWCNT/**8**, in which sizable shifts of electron density prevail, is followed by a full separation of charges, namely oxidation of exTTF and reduction of CoMoCAT SWCNT. By following the characteristics of the oxidized exTTF[31] and the reduced CoMoCAT SWCNT,[24,32] we deduce a lifetime of the electron transfer product of 160 ps.[33]

Finally, we probed MWCNT/**8**. Here, upon photoexcitation only, broad and nearly featureless transient bleach is seen in the near-infrared. Within 5 ps a spectrum develops that in the visible bears great resemblance with what has been seen for CoMoCAT SWCNT/**8**. In particular, the signature of the one-electron oxidized radical cation of exTTF is visible at 640 nm. In the near-infrared region, on the other hand, only a broad transient with a minimum around 1150 nm is formed concomitantly. Fitting the visible and near-infrared features brings an electron transfer product lifetime of around 380 ps to light (Figure 11).

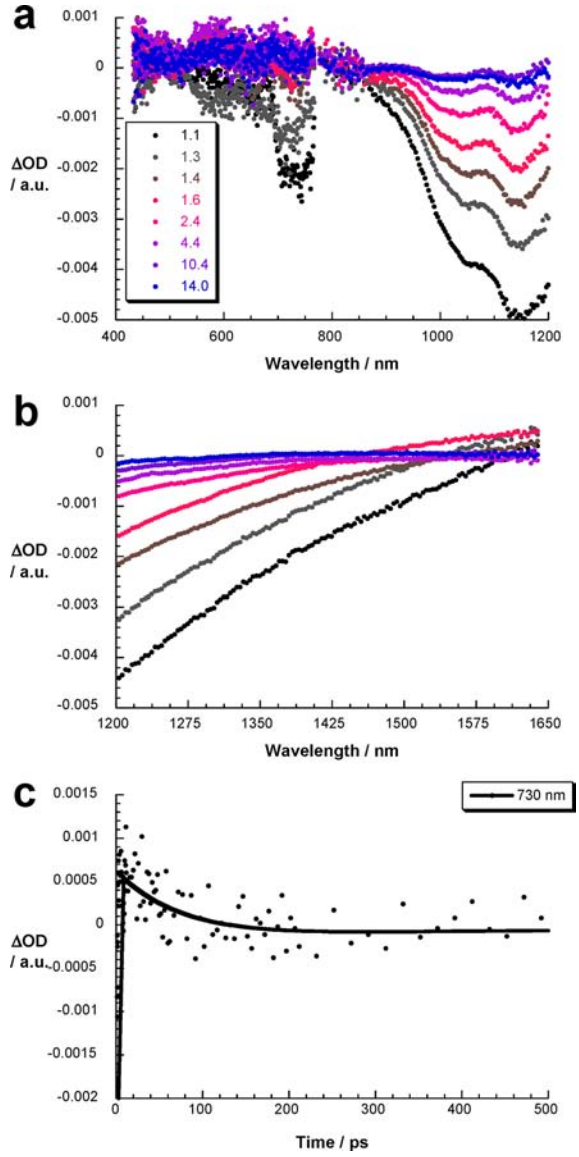

Figure 10. (a) Differential absorption spectra (visible and near-infrared) obtained upon femtosecond pump probe experiments (387 nm) of CoMoCAT SWCNT/**8** in D_2O with several time delays between 0 and 14 ps at room temperature. (b) Differential absorption spectra (extended near-infrared) obtained upon femtosecond pump probe experiments (387 nm) of CoMoCAT SWCNT/**8** in D_2O with several time delays between 0 and 14 ps at room temperature. (c) Time absorption profile of the spectra shown in the upper part at 730 nm monitoring the electron transfer.

■ CONCLUSIONS

On the basis of a synthetically straightforward nanotweezers design, we have prepared a new exTTF-based receptor that combines the synergy of $\pi-\pi$ stacking and/or electron donor–acceptor interactions with a versatile second generation dendron that carries terminal carboxylic groups. In fact, deprotonation of the latter rendered the exTTF nanotweezers fully water-soluble as a prerequisite to disperse CNT in aqueous media.

Moreover, we have demonstrated the ability of exTTF nanotweezers **8** to suspend CNT of different diameters, as confirmed by TEM and AFM measurements. Most importantly, steady-state and time-resolved measurements were used to probe the electronic communication between CNT and **8** in the ground and in the excited states. To this end, irradiation of CoMoCAT SWCNT/**8** and MWCNT/**8** with visible light reflects the interaction in terms of a thermodynamically driven electron transfer. Figure 12 sketches the energy diagrams for the dominant CoMoCAT SWCNT, that is, (7,5) and (7,6). In fact, the different driving forces of 0.53 eV for (7,5) and 0.33 eV

dx.doi.org/10.1021/ja211362z | J. Am. Chem. Soc. 2012, 134, 9183–9192

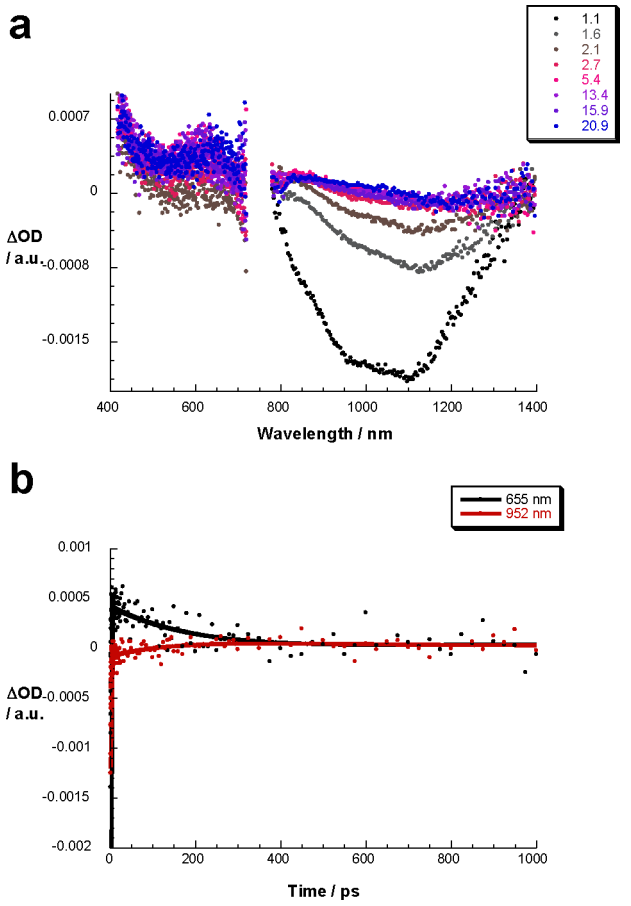

Figure 11. (a) Differential absorption spectra (visible and near-infrared) obtained upon femtosecond pump probe experiments (387 nm) of MWCNT/**8** in D_2O with several time delays between 0 and 20.9 ps at room temperature. (b) Time absorption profiles of the spectra shown in the upper part at 655 nm (black spectrum) and 952 nm (red spectrum) monitoring the electron transfer.

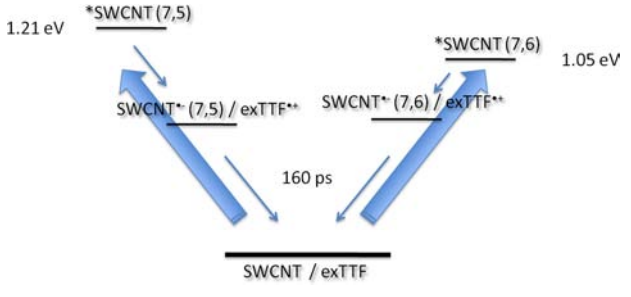

Figure 12. Energy diagram of CoMoCAT SWCNT—(7,5) and (7,6)—upon excitation at 387 nm.

for (7,6) are reflected in fluorescence quenching factors of 108 and 84, respectively. Regardless of (7,5) or (7,6), the electron transfer product exhibited similar energies and indistinguishable back electron transfer dynamics, as well as a quantum efficiency of 0.99.

At first glance, the corresponding electron transfer products in CoMoCAT SWCNT/**8** and MWCNT/**8** seemed nearly identical, with lifetimes of several hundred picoseconds. A closer look reveals that the presence of several concentric nanotubes in, for example, MWCNT is, however, beneficial in prolonging the lifetime of the charge separated radical ion pair state. In the case of HiPco SWCNT/**8**, no clear-cut evidence was gathered that corroborates the formation of an electron transfer product, despite strong electronic communication in the ground and excited states in the form of red-shifted absorption and strongly quenched SWCNT fluorescence, respectively.

The present study pioneers a straightforward methodology to design novel and versatile electroactive receptors able to interact and immobilize CNT of different physical and electronic features in water. In addition, our investigations prompt future use of receptors that, on one hand, feature chiral angle selective recognition of SWCNT and, on the other hand, could potentially be applied in the area of photovoltaics.

EXPERIMENTAL SECTION

Materials. SWCNT were obtained from Unidym Inc. (Purified HiPCo SWCNT batch number P0343) and SouthWest Nanotechnologies (CoMoCAT SWCNT batch number SG65-0012). MWCNT were obtained from Future Carbon (batch number CNT09120262-1). All chemicals were purchased from chemical suppliers and used without further purification. All analytical reagent-grade solvents were purified by distillation.

Characterization. Thin layer chromatography (TLC): Riedel-de Haën silica gel F254, Merck silica gel 60 F254, and UV-lamp detection. Column chromatography: MN silica gel 60 M (230−440 mesh, 0.04−0.063 nm). IR spectroscopy: Bruker FT-IR Vector 22 with an ATR RFS 100/S unit; substances were measured as solids or liquids. Mass spectrometry: Shimadzu AXIMA Confidence or HP 5989a with a time-of-flight mass spectrometer with a 337 nm nitrogen laser; sinapic acid (SIN) and *trans*-2-[3-(4-*tert*-butylphenyl)-2-methyl-2-propenylidene]malononitrile (DCTB) were used as matrices. NMR spectroscopy: JEOL JNM GX 400, Bruker Avance 400, and Bruker Avance 300. Chemical shifts are given in ppm relative to TMS. Resonance multiplicities are indicated as s (singlet), d (doublet), t (triplet), q (quartet), and m (multiplet); nonresolved and broad resonances as br. The raw data were processed with a demo-version of MestReNova 7.

TEM Analysis. TEM measurements were performed on a PHILIPS CM 300 UT high-resolution transmission electron microscope (300 kV acceleration voltage, 0.172 nm point resolution—Scherzer focus) equipped with a 2 camera system (TV System and CCD camera) and EM900 from Carl Zeiss AG. Samples for TEM were prepared by casting one drop of the sample solution onto a standard Formvar film on a copper grid or on a holey carbon grid and washing with water.

AFM Analysis. Atomic force microscopy was performed on a SPM Nanoscope IIIa multimode microscope working in tapping mode with a RTESPA tip (Veeco) at a working frequency of ∼235 kHz. The samples were prepared by drop casting on silicon wafers from a solution of the exTTF-tweezers/SWCNT in borax solution 0.1 M and washed with deionized water afterward.

Photophysical Measurements. Steady-state UV/vis/NIR absorption spectroscopy was performed on a Cary 5000 spectrometer (Varian). Transient absorption spectroscopy was performed with 775 and 387 nm laser pulses from an amplified Ti/sapphire laser system (ModelCPA2101, Clark-MXR Inc.; output: 775 nm, 1 kHz, and 150 fs pulse width) in the TAPPS (transient absorption pump/probe system) Helios from Ultrafast Systems with 200 nJ laser energy. Steady-state fluorescence spectra were taken from samples with a FluoroMax3 spectrometer (Horiba) in the visible detection range and with a FluoroLog3 spectrometer (Horiba) with a IGA Symphony (5121 1 μm) detector in the NIR detection range. The spectra were recorded with a FT-Raman spectrometer RFS100 (Bruker), and a FluoroLog3 spectrometer (Horiba) with a IGA Symphony detector in the NIR detection range.

Synthetic Details. Compounds **1**,[25] **2**, **3**, **4**,[26] and **6**[27] were prepared according to previously reported synthetic procedures and showed identical spectroscopic properties to those reported therein.

1,3-Bis{(9,10-di(1,3-dithiol-2-yliden)-9,10-dihydroanthracen-2-yl)methyl}-5-((*tert*-butoxycarbonyl)methoxy) Isophthalate

dx.doi.org/10.1021/ja211362z | *J. Am. Chem. Soc.* 2012, 134, 9183−9192

(5). 94 mg of **4**[26] (0.10 mmol) and 29 μL of *tert*-butylbromoacetate (37 mg, 0.19 mmol) was dissolved in 50 mL of acetone. After the addition of 40 mg of K_2CO_3 (0.29 mmol), the suspension was heated to reflux for 5 h. Afterward, water was added to dissolve the excess of K_2CO_3, the mixture was extracted three times with CH_2Cl_2, and the organic phases were dried over $MgSO_4$. The product was purified via column chromatography on silica with CH_2Cl_2/EtOAc 95:5 and isolated as a yellow solid in 84% yield (0.09 mmol, 91 mg). ^{1}H NMR ($CDCl_3$, 300 MHz, 298 K) δ 1.36 (s, 9H), 4.51 (s, 2H), 5.33 (s, 4H), 6.14 (m, 8H), 7.21 (m, 6H), 7.59 (m, 6H), 7.74 (m, 4H), 8.44 (s, 1H); ^{13}C NMR ($CDCl_3$, 75 MHz, 298 K) δ 28.39, 66.30, 67.43, 83.26, 117.33, 117.58, 117.87, 120.61, 121.82, 125.34, 125.57, 125.91, 126.35, 126.43, 132.34, 133.61, 135.65, 135.80, 136.21, 158.37, 162.73, 165.68, 167.64; FTIR (neat): 802, 1157, 1228, 1295, 1554, 1595, 1675, 1725, 2852, 2924, 3077 cm^{-1}. UV−vis (CH_2Cl_2): λ_{max} 365, 432, 484 (sh) nm. MALDI-TOF *m*/*z*: 1081 $[M]^+$, 1025 $[M\text{-}t\text{Bu}]^+$.

1,3-Bis{(9,10-di(1,3-dithiol-2-yliden)-9,10-dihydroanthracen-2-yl)methyl}-5-(*tert*-butyl Protected 2G-Newkome Cendron) Isophthalate (7). 91 mg of **5** (0.09 mmol) was dissolved in 20 mL of formic acid and stirred at room temperature for 12 h. After the acid was removed by distillation *in vacuo*, the residue was dissolved in 50 mL of DMF and cooled in an ice bath. Following that, 35 mg of DCC (0.17 mmol), 23 mg of HOBt (0.17 mmol), and 1 mg of DMAP (8.40 μmol) were added, and the solution was stirred for 30 min at 0 °C. Afterward, 241 mg of NH_2-*tert*-butyl protected 2G-Newkome dendron **6**[27] (0.17 mmol) was added, and the reaction was allowed to proceed for three days at room temperature. After purification by column chromatography on silica with CH_2Cl_2/EtOAc 1:1, the product was obtained as a yellow solid in 55% yield (0.05 mmol, 123 mg). ^{1}H NMR ($CDCl_3$, 400 MHz, 298 K) δ 1.37 (s, 81H), 1.91 (m, 24H), 2.15 (m, 24H), 4.73 (m, 2H), 5.39 (m, 4H), 6.17 (m, 3H), 6.26 (m, 8H), 7.64 (m, 7H), 7.82 (m, 8H), 7.32 (m, 7H), 7.67 (m, 6H), 7.82 (m, 4H), 8.50 (m, 1 H); ^{13}C NMR ($CDCl_3$, 100 MHz, 298 K) δ 28.05, 29.73, 31.33, 55.73, 57.47, 57.88, 66.98, 80.49, 116.90, 117.14, 117.46, 120.24, 120.35, 120.52, 121.40, 121.76, 124.22, 124.64, 125.90, 125.09, 125.46, 125.91, 126.00, 126.50, 127.27, 127.87, 131.81, 131.97, 132.09, 133.23, 135.23, 135.37, 135.79, 156.69, 158.09, 165.29, 165.43, 166.68, 172.27, 172.64; FTIR (neat): 750, 763, 1153, 1260, 1275, 1456, 1574, 1627, 1726, 2360, 2852, 2927, 3005 cm^{-1}. UV−vis (CH_2Cl_2): λ_{max} 366, 433, 485 (sh) nm. MALDI-TOF (DCTB) *m*/*z*: 2445 $[M]^+$.

1,3-Bis{(9,10-di(1,3-dithiol-2-yliden)-9,10-dihydroanthracen-2-yl)methyl}-5-(2G-Newkome dendron) Isophthalate (8). 115 mg of **7** (0.05 mmol) was dissolved in 20 mL of formic acid and stirred at room temperature for three days. The solvent was evaporated and the product was dried *in vacuo* to give a yellow solid in 99% yield (0.05 mmol, 90 mg). ^{1}H NMR (DMSO-d_7/D_2O 2:1, 400 MHz, 298 K) δ 1.70−1.95 (br m, 48H), 4.53 (br s, 2H), 5.50 (br m, 4H), 7.29−8.18 (br m, 17 H); ^{13}C NMR (DMSO-d_7/D_2O 2:1, 100 MHz, 298 K) δ 31.01, 33.17, 133.45, 162.19; FTIR (neat): 750, 764, 992, 1026, 1260, 1275, 1458, 1573, 1625, 2360, 2851, 2928, 2989, 3006 cm^{-1}. UV−vis (H_2O): λ_{max}373, 440, 507 (sh) nm. MALDI-TOF (SIN) *m*/*z*: 1966 $[M + Na]^+$, 1942 $[M]^+$.

■ ASSOCIATED CONTENT

Ⓢ Supporting Information

Supplementary Figures S1−S9 as indicated in the text. This material is available free of charge via the Internet at http://pubs.acs.org.

■ AUTHOR INFORMATION

Corresponding Author

andreas.hirsch@chemie.uni-erlangen.de; guldi@chemie.uni-erlangen.de; nazmar@quim.ucm.es

Notes

The authors declare no competing financial interest.

■ ACKNOWLEDGMENTS

We thank G. Fernández, E. M. Pérez, and L. Sánchez for their helpful advice in the synthesis of the exTTF-tweezers. We appreciate the help of Dr. Vito Sgobba and Georgios Katsukis with the TEM measurement. Financial support by the MICINN of Spain (CTQ2011-24652, PIB2010JP-00196, and CSD2007-00010), FUNMOLS (FP7-212942-1), the CAM (MADRISOLAR-2 S2009/PPQ-1533), the Cluster of Excellence "Engineering of Advanced Materials", ICMM, ZMP "Zentralinstitut für Neue Materialien und Prozesstechnik", FCI, the Office of Basic Energy Sciences of the U.S., and the Sonderforschungsbereich 953 "Synthetic Carbon Allotropes" is gratefully acknowledged.

■ REFERENCES

(1) (a) Reich, S.; Thomsen, C.; Maultzsch, J. *Carbon Nanotubes: Basic Concepts and Physical Properties*; VCH: Weinheim, Germany; 2004. (b) Popov, V. N.; Lambin, P. *Carbon Nanotubes*; Springer: Dordrecht, 2006. (c) Guldi, D. M.; Martín, N. *Carbon Nanotubes and Related Structures*; VCH: Weinheim, Germany, 2010. (d) Akasaka, T.; Wudl, F.; Nagase, S. *Chemistry of Nanocarbons*; John Wiley & Sons: Chichester, United Kingdom, 2010.

(2) Prato, M. *Nature* **2010**, *465*, 172.

(3) (a) Shulaker, M. M.; Wei, H.; Patil, N.; Provine, J.; Chen, H.-Y.; Wong, H.-S. P.; Mitra, S. *Nano Lett.* **2011**, *11*, 1881. (b) Kim, T. H.; Lee, B. Y.; Jaworski, J.; Yokoyama, K.; Chung, W.-J.; Wang, E.; Hong, S.; Majumdar, A.; Lee, S.-W. *ACS Nano* **2011**, *5*, 2824.

(4) Wang, S.; Zeng, Q.-S.; Yang, L.-J.; Zhang, Z.-Y.; Wang, Z.-X.; Pei, T.; Ding, L.; Liang, X.-L.; Gao, M.; Li, Y.; Peng, L.-M. *Nano Lett.* **2011**, *11*, 23.

(5) (a) Lee, J. M.; Park, J. S.; Lee, S. H.; Kim, H.; Yoo, S.; Kim, S. O. *Adv. Mater.* **2011**, *23*, 629. (b) Holt, J. M.; Ferguson, A. J.; Kopidakis, N.; Larsen, B. A.; Bult, J.; Rumbles, G.; Blackburn, J. L. *Nano Lett.* **2010**, *10*, 4627. (c) Barnes, T. M.; Bergeson, J. D.; Tenent, R. C.; Larsen, B. A.; Teeter, G.; Jones, K. M.; Blackburn, J. L.; van de Lagemaat. *J. Appl. Phys. Lett.* **2010**, *96*, 243309.

(6) Toma, F. M.; Sartorel, A.; Iurlo, M.; Carraro, M.; Parisse, P.; Maccato, C.; Rapino, S.; Gonzalez, B. R.; Amenitsch, H.; Da Ros, T.; Casalis, L.; Goldoni, A.; Marcaccio, M.; Scorrano, G.; Scoles, G.; Paolucci, F.; Prato, M.; Bonchio, M. *Nature Chem.* **2010**, *2*, 826.

(7) Wang, F.; Swager, T. M. *J. Am. Chem. Soc.* **2011**, *133*, 11181.

(8) (a) Liu, B.; McCarthy, M. A.; Rinzler, A. G. *Adv. Funct. Mater.* **2010**, *20*, 3440. (b) Brunel, D.; Mayer, A.; Melin, T. *ACS Nano* **2010**, *4*, 5978.

(9) (a) Tung, V. C.; Chen, L.-M.; Allen, M. J.; Wassei, J. K.; Nelson, K.; Kaner, R. B.; Yang, Y. *Nano Lett.* **2009**, *9*, 1949. (b) Ferris, C. J.; in het Panhuis, M. *Soft Matter* **2009**, *5*, 1466. (c) Hayashi, T.; Kim, Y. A.; Natsuki, T.; Endo, M. *ChemPhysChem* **2007**, *8*, 999.

(10) For recent reviews, see: (a) Peng, X.; Wong, S. S. *Adv. Mater.* **2009**, *21*, 625. (b) Singh, P.; Campidelli, S.; Giordani, S.; Bonifazi, D.; Bianco, A; Prato, M. *Chem. Soc. Rev.* **2009**, *38*, 2214. (c) Zhao, Y. L; Stoddart, J. F. *Acc. Chem. Res.* **2009**, *42*, 116. (d) Wang, H. *Curr. Opin. Colloid Interface Sci.* **2009**, *14*, 364. (e) Eder, D. *Chem. Rev.* **2010**, *110*, 1348. (f) Karousis, N.; Tagmatarchis, N.; Tasis, D. *Chem. Rev.* **2010**, *110*, 5366. (g) Hirsch, A. *Nat. Mater.* **2010**, *9*, 868.

(11) (a) Zhang, Z.; Che, Y.; Smaldone, R. A.; Xu, M.; Bunes, B. R.; Moore, J. S.; Zang, L. *J. Am. Chem. Soc.* **2010**, *132*, 14113. (b) Sprafke, J. K.; Stranks, S. D.; Warner, J. H.; Nicholas, R. J.; Anderson, H. L. *Angew. Chem., Int. Ed.* **2011**, *50*, 2313. (c) Bartelmess, J.; Ehli, C.; Cid, J. J.; García-Iglesias, M.; Vázquez, P.; Torres, T.; Guldi, D. M. *Chem. Sci.* **2011**, *2*, 652. (d) Llanes-Pallas, A.; Yoosaf, K.; Traboulsi, H.; Mohanraj, J.; Seldrum, T.; Dumont, J.; Minoia, A.; Lazzaroni, R.; Armaroli, N.; Bonifazi, D. *J. Am. Chem. Soc.* **2011**, *133*, 15412.

(12) Bergin, S. D.; Nicolosi, V.; Streich, P. V.; Giordani, S.; Sun, Z.; Windle, A. H.; Ryan, P.; Niraj, N. P. P.; Wang, Z.-T. T.; Carpenter, L.; Blau, W. J.; Boland, J. J.; Hamilton, J. P.; Coleman, J. N. *Adv. Mater.* **2008**, *20*, 1876.

(13) (a) Simmons, J. M.; In, I.; Campbell, V. E.; Mark, T. J.; Léonard, F.; Gopalan, P. M.; Eriksson, P. *Phys. Rev. Lett.* **2007**, *98*, 086802. (b) Backes, C.; Schmidt, C. D.; Hauke, F.; Böttcher, C.; Hirsch, A. *J. Am. Chem. Soc.* **2009**, *131*, 2172. (c) Bartelmess, J.; Ballesteros, B.; de la Torre, G.; KIessling, D.; Campidelli, S.; Prato, M.; Torres, T.; Guldi, D. M. *J. Am. Chem. Soc.* **2010**, *132*, 16202.
(14) (a) Stranks, S. D.; Sprafke, J. K.; Anderson, H. L.; Nicholas, R. J. *ACS Nano* **2011**, *5*, 2307. (b) Lemasson, F. A.; Strunk, T.; Gerstel, P.; Hennrich, F.; Lebedkin, S.; Barner-Kowollik, C.; Wenzel, W.; Kappes, M. M.; Mayor, M. *J. Am. Chem. Soc.* **2011**, *133*, 652. (c) Ozawa, H.; Fujigaya, T.; Niidome, Y.; Hotta, N.; Fujiki, M.; Nakashima, N. *J. Am. Chem. Soc.* **2011**, *133*, 2651. (d) Lemasson, F.; Tittmann, J.; Hennrich, F.; Stürzl, N.; Malik, S.; Kappes, M. M.; Mayor, M. *Chem. Commun.* **2011**, *47*, 7428.
(15) Tromp, R. M.; Afzali, A.; Freitag, M.; Mitzi, D. B.; Chen, Z. *Nano Lett.* **2008**, *8*, 469.
(16) Marquis, R.; Kulikiewicz, K.; Lebedkin, S.; Kappes, M. M.; Mioskowski, C.; Meurier, S.; Wagner, A. *Chem.—Eur. J.* **2009**, *15*, 11187.
(17) Mustafizur Rahman, A. F. M.; Wang, F.; Matsuda, K.; Kimura, T.; Komatsu, N. *Chem. Sci.* **2011**, *2*, 862.
(18) (a) Peng, X.; Komatsu, N.; Bhattachary, S.; Shimawaki, T.; Aonuma, S.; Kimura, T.; Osuka, A. *Nature Nanotechnol.* **2007**, *2*, 361. (b) Peng, X.; Komatsu, N.; Kimura, T.; Osuka, A. *J. Am. Chem. Soc.* **2007**, *129*, 15947. (c) Peng, X.; Komatsu, N.; Kimura, T.; Osuka, A. *ACS Nano* **2008**, *2*, 2045.
(19) Wang, F.; Matsuda, K.; Mustafizur Rahman, A. F. M.; Peng, X.; Kimura, T.; Komatsu, N. *J. Am. Chem. Soc.* **2010**, *132*, 10876.
(20) (a) Ehli, C.; Oelsner, C.; Guldi, D. M.; Mateo-Alonso, M.; Prato, M.; Schmidt, C.; Backes, C.; Hauke; Hirsch, A. *Nature Chem.* **2009**, *1*, 243. (b) Backes, C.; Schmidt, C. D.; Rosenlehner, K.; Hauke, F.; Coleman, J. N.; Hirsch, A. *Adv. Mater.* **2010**, *22*, 788. (c) Backes, C.; Karabudak, E.; Schmidt, C. D.; Hauke, F.; Hirsch, A.; Wohlleben, W. *Chem.—Eur. J.* **2010**, *16*, 13176. (d) Backes, C.; Mundloch, U.; Schmidt, C. D.; Coleman, J. N.; Wohlleben, W.; Hauke, F.; Hirsch, A. *Chem.—Eur. J.* **2010**, *16*, 13185. (e) Oelsner, C.; Schmidt, C.; Hauke, F.; Prato, M.; Hirsch, A.; Guldi, D. M. *J. Am. Chem. Soc.* **2011**, *133*, 4580. (f) Backes, C.; Schunk, T.; Hauke, F.; Hirsch, A. *J. Mater. Chem.* **2011**, *21*, 3554.
(21) Backes, C.; Schmidt, C. D.; Hauke, F.; Hirsch, A. *Chem. Asian J.* **2011**, *6*, 438.
(22) For recent reviews about TTF derivatives, see: (a) Martín, N.; Sánchez, L.; Herranz, M. A.; Illescas, B.; Guldi, D. M. *Acc. Chem. Res.* **2007**, *40*, 1015. (b) Canevet, D.; Salle, M.; Zhang, G.; Zhang, D.; Zhu, D. *Chem. Commun.* **2009**, 2245. (c) Pérez, E. M.; Illescas, B. M.; Herranz, M. A.; Martín, N. *New J. Chem.* **2009**, *33*, 228. (d) Brunetti, F. G.; López, J. L.; Atienza, C.; Martín, N. *J. Mater. Chem.* **2012**, *22*, 4188.
(23) (a) Pérez, E. M.; Sánchez, L.; Fernández, G.; Martín, N. *J. Am. Chem. Soc.* **2006**, *128*, 7172. (b) Pérez, E. M.; Martín, N. *Chem. Soc. Rev.* **2008**, *37*, 1512. (c) Pérez, E. M.; Martín, N. *Pure Appl. Chem.* **2010**, *82*, 523.
(24) Herranz, M. A.; Ehli, C.; Campidelli, S.; Gutiérrez, M.; Hug, G. L.; Ohkubo, K.; Fukuzumi, S.; Prato, M.; Martín, N.; Guldi, D. M. *J. Am. Chem. Soc.* **2008**, *130*, 66.
(25) Marshallsay, G. J.; Bryce, M. R. *J. Org. Chem.* **1994**, *59*, 6847.
(26) Fernández, G.; Pérez, E. M.; Sánchez, L.; Martín, N. *Angew. Chem., Int. Ed.* **2008**, *47*, 1094.
(27) (a) Newkome, G. R.; Behera, R. K.; Moorefield, C. N.; Baker, G. R. *J. Org. Chem.* **1991**, *56*, 7162. (b) Newkome, G. R.; Weis, C. D. *Org. Prep. Proced. Int.* **1996**, *28*, 495. (c) Brettreich, M.; Hirsch, A. *Synlett* **1998**, *12*, 1396.
(28) Bachilo, S. M.; Strano, M. S.; Kittrell, C.; Hauge, R. H.; Smalley, R. E.; Weisman, R. B. *Science* **2002**, *298*, 2361.
(29) (a) Graupner, R. *J. Raman Spectrosc.* **2007**, *38*, 673. (b) Dresselhaus, M. S.; Dresselhaus, G.; Jorio, A.; Souza Filho, A. G.; Pimenta, M. A.; Saito, R. *Acc. Chem. Res.* **2002**, *35*, 1070.
(30) Park, J.; Deria, P.; Therien, M. J. *J. Am. Chem. Soc.* **2011**, *133*, 17156.
(31) Guldi, D. M.; Sánchez, l.; Martín, N. *J. Phys. Chem. B* **2001**, *105*, 7139.
(32) Hahn, U.; Engmann, S.; Oelsner, C.; Ehli, C.; Guldi, D. M.; Torres, T. *J. Am. Chem. Soc.* **2010**, *132*, 6392.
(33) Corresponding experiments at 778 nm lead to lifetimes of 196 ps for CoMoCAT SWCNT/**8** and of 146 ps for HiPco SWCNT/**8**.